

The origin and structure of clumps along molecular outflows: the test case of CB3

Serena Viti,^{1,2*} Claudio Codella,³ Milena Benedettini,¹ Rafael Bachiller⁴

¹ CNR-Istituto di Fisica dello Spazio Interplanetario, Area di Ricerca di Tor Vergata, via del Fosso del Cavaliere 100, I-00133, Roma, Italy

² Department of Physics and Astronomy, University College London, Gower Street, London, WC1E 6BT, UK

³ Istituto di Radioastronomia, CNR, Sezione di Firenze, Largo E. Fermi 5, 50125 Firenze, Italy

⁴ IGN Observatorio Astronómico Nacional, Apartado 1143, 28800 Alcalá de Henares, Spain

Received ; accepted

ABSTRACT

We investigate the origin of the small, chemically rich molecular clumps observed along the main axis of chemically rich outflows such as CB3 and L1157. We develop a chemical model where we explore the chemical evolution of these clumps, assuming they are partially pre-existing to the outflow, or alternatively newly formed by the impact of the outflow on the surrounding medium. The effects of the impact of the outflow are reproduced by density and temperature changes in the clump. We find that the observed abundances of CH₃OH, SO and SO₂ are best reproduced by assuming a scenario where the dense molecular gas observed is probably pre-existing in the interstellar medium before the formation of their exciting (proto)stars and that the clumpiness and the rich chemistry of the clumps are a consequence of a pre-existing density enhancement and of its interaction with the outflow.

Key words: ISM: clouds - ISM: jets and outflows - ISM: molecules - ISM: individual objects: CB3 - ISM: individual objects: L1157

1 INTRODUCTION

At an early stage in their evolution stars eject material in the form of outflows. In fact, the first signs of an outflow are coupled with infall motion and therefore with the first stages of star formation (e.g. Bachiller 1996; Richer et al. 2000). Once the protostar is formed, outflows are the main means of removing the material left over from the collapse of the cloud.

Small molecular clumps (~ 0.1 pc) are detected in association with several outflows; it is generally believed that the clumps are generated by episodic mass loss of the forming object. To date, there is no detailed understanding of the role of the clumpiness in outflows. In fact, two main kinds of clumps have been observed: (i) high-velocity clumps or the so-called molecular bullets which are well defined entities travelling at velocities larger than 100 km s⁻¹. The prototype is L1448 (Bachiller, Martín-Pintado & Fuente 1991), where bullets appear in pairs with the members of a pair being symmetric in both position and velocity with respect to the star. These bullets are most likely associated with mini-bow shocks formed by the outflow propagation (e.g. Dutrey, Guilloteau & Bachiller 1997). The molecular lines

emitted by this kind of clump are relatively weak, so their chemical composition remains unknown. (ii) A second kind of clump, observed along a few outflows associated with low- and intermediate-mass stars; these outflows stand out because of their association with chemically rich clumps at definitely lower velocity, such as L1157, BHR71, and CB3 (Bourke et al. 1997; Codella & Bachiller 1999; Bachiller et al. 2001). The origin of these chemically rich clumps is not yet clear.

In this paper, we investigate the origin and nature of the second kind of clumps by the use of a chemical model that simulates the clump formation and its subsequent interaction with the outflow. We consider here two main scenarios: (1) pre-existing clumps, affected by the outflow, and (2) newly-formed clumps, created by the outflow. *Note that we will use the word pre-existing to indicate a density structure formed before the advent of the outflow.* Our definition does not imply that the observed abundances (e.g Codella & Bachiller 1999; Bachiller et al. 2001) are pre-existing to the outflow.

In what follows, we introduce our two scenarios for the formation of the clumps.

(1) The clumps are pre-existing to the outflow; for example they may be either remnant material of the collapsing parent cloud or completely independent of the star formation

* E-mail: sv@star.ucl.ac.uk

process, but present homogeneously in the dark molecular cloud (e.g. Falle & Hartquist 2002; Morata et al. 2003; Garrod et al. 2003). In this scenario, we observe these clumps in association with molecular outflows because, as the outflows travel through the molecular cloud, they interact with the clumps and shock them. If this is the case, then the clumps may not be an indication of the episodic nature of outflows. (2) The cloud material is homogeneous and low in density but as an episodic outflow forms, its interaction with the surrounding homogeneous material will lead to a compression (increase in density) and increase in temperature (with subsequent evaporation of the grains mantles) in localized regions *only*, hence the observed clumpiness (e.g. Arce & Goodman 2001, 2002, and reference therein). In this scenario, the clumps are a direct manifestation of the episodic nature of outflows.

Note that these scenarios do not necessarily exclude each other: in fact, the morphology of the regions where outflows and jets propagate have a very complicated geometry and structure by their very nature (e.g. Hester et al. 1998).

The main aim of this study is to investigate the nature of the chemically rich clumps by modelling their chemical evolution and by comparing the models with observations. In particular, we attempt to identify discriminants between the two scenarios. In this paper, we will focus our attention on the clumps located in the intermediate-mass star forming region CB3 (Codella & Bachiller 1999). In addition, a low mass case, represented by the L1157 outflow, will be briefly discussed. Our model is described in Section 2, and our results are presented, discussed and compared with observations in Section 3. A brief conclusion is given in Section 4.

2 THE MODEL

The aim of the modelling is to explore the chemistry in the different scenarios of clump formation described above. The basic chemical model we adopt is a modification of the time-dependent model employed in Viti & Williams (1999) and Viti et al. (2003). The chemical network is taken from the UMIST database (Millar et al. 1997; Le Teuff et al. 2000). We follow the chemical evolution of 221 species involved in 3194 gas-phase and grain reactions. Our model is two-phase calculation. Phase I represents the formation of the pre-existing clumps, Scenario 1, or of the homogeneous dark cloud, Scenario 2, from diffuse gas, while Phase II represents the effect on the gas and dust of the outflow. Figure 1 shows a schematic of how the two scenarios are treated in the model.

In Phase I, we allow the diffuse gas to collapse gravitationally within the molecular cloud. During the collapse phase, gas-phase chemistry and freeze-out on to dust grains with subsequent processing are assumed to occur. The initial density of the gas is taken to be 100 cm^{-3} , and the final density is treated as a free parameter (see later). During Phase I, the temperature is kept constant at 10 K. In Phase II we simulate the presence of the outflow (see Sections 2.1–2.3 for a detailed description of each grid of models) by an increase in temperature and an assumed subsequent thermal or (non-dissociative) shock-induced evaporation of the

grain mantles. Sputtering of the core of the grains and fast, dissociative shocks are not included. Phase II was halted at 10^5 yr .

In Phase II, Scenario 1, we have investigated both a uniform and homogeneous clump (the set of physical parameters for which we have explored the chemistry is here called Grid A), and clumps with a density structure (Grids B and C). We have also considered the possibilities that after the initial increase of the temperature (to $\sim 100 \text{ K}$), the temperature remains constant (Grid C) or enters a shocked phase to a higher temperature, followed by cooling (Grid B). See 2.1–2.3 for more details.

In Scenario 2 the outflow impacts on a dark molecular cloud, of density $\sim 10^4 \text{ cm}^{-3}$, and induces the formation of clumps. In this case we use Phase I of the model to simulate the formation of the dark cloud, and Phase II to simulate the formation of the clumps due to the impact of the outflow. During Phase II, the gas and dust temperatures increase as the clump forms, and the grains evaporate. Here too we investigated the possibility that after the initial increase to 100 K, the temperature enters a shocked phase to a higher temperature and subsequent cooling. This scenario will be modelled in a range of physical parameters here labelled Grid D.

Within each grid we have explored a reasonably large parameter space. To impose some constraints to the initial parameters, we adopt the physical parameters derived by Codella & Bachiller (1999) for the clumps observed along CB3, namely: a size for the final clump of $\sim 0.12 \text{ pc}$, a final density of about $10^5\text{--}10^6 \text{ cm}^{-3}$, a final temperature of 100 K, and an age of 10^5 yrs .

2.1 Scenario 1: Grid A

Table 1 lists the details for the models computed for Grid A. Grid A consists of 9 models where, in Phase I, we vary the following parameters: i) the type of collapse, ii) the depletion efficiency, iii) the final density, and iv) the initial sulphur elemental abundance.

The collapse is either treated as free-fall as described by Rawlings et al. (1992) or retarded.

The depletion efficiency is determined by what fraction of the gas phase material is frozen on to the grains, and undergoes hydrogenation. Several routes of hydrogenation for the most significant species (O, N, C, CO) have been explored. The freeze-out fraction is arranged by adjusting the grain surface area per unit volume, and assumes a sticking probability of unity for all species. The fraction of material on grains is then dependent on the product of the sticking probability and the amount of cross section provided per unit volume by the adopted grain size distribution. This product was varied so that at the end of Phase I, we would have different percentages of ices (see Table 1). Note that as the chemistry is time-dependent, different species form at different times and as a consequence the material frozen out on the grains at any one time is *not* representative of the whole gas but of selected species (in this case, we chose to monitor frozen CO).

For the final density, we chose a lower limit of 10^5 cm^{-3} and an upper limit of $5 \times 10^6 \text{ cm}^{-3}$.

The initial relative abundance of sulphur is very uncertain (e.g., Ruffle et al. 1999); we chose the solar value as

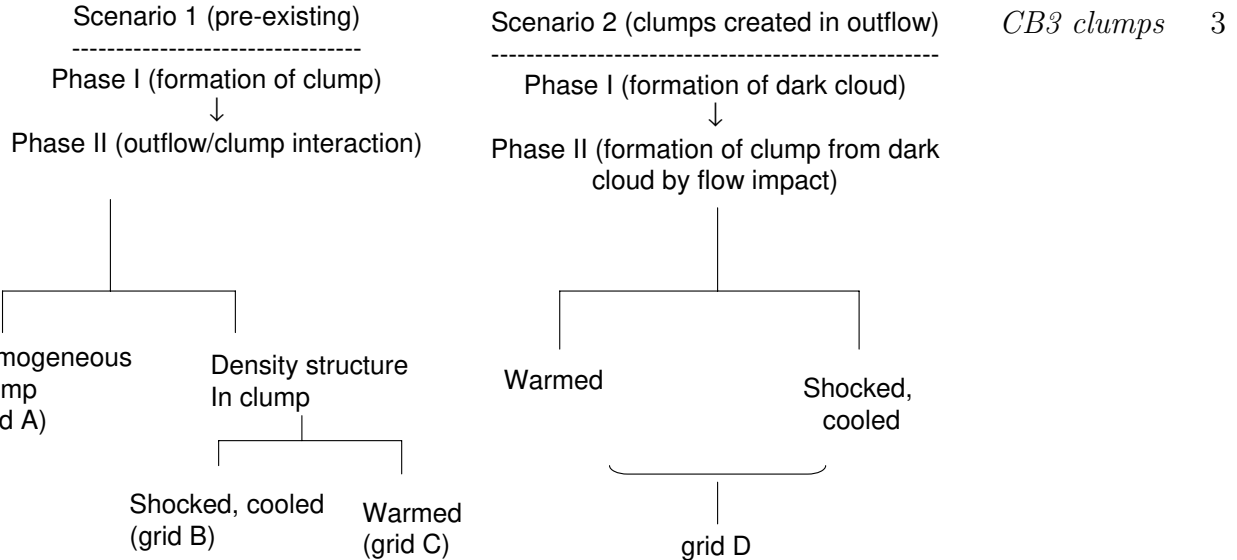


Figure 1. A flow diagram of the two Scenarios as treated by the chemical model (see Section 2).

Table 1. Model Parameters for Grid A. The notation $a(b)$ signifies $a \times 10^b$. The model number is listed in Column 1; Column 2 shows the density of the gas; Column 3, 4 and 5 shows respectively the percentage of the gas depleted onto grain at the end of Phase I, the type of collapse (B=1 free-fall; B=0.1 retarded), the initial sulphur abundance.

Model	n_f (cm^{-3})	Depletion (%)	B	Sulphur
A1	1(5)	15	1.0	1.3(-5)
A2	1(5)	35	0.1	1.3(-5)
A3	1(5)	11	0.1	1.3(-5)
A4	1(5)	20	1.0	1.9(-6)
A5	1(6)	20	1.0	1.3(-5)
A6	1(6)	30	1.0	1.3(-7)
A7	1(6)	55	1.0	1.3(-7)
A8	1(6)	80	1.0	1.3(-7)
A9	5(6)	25	1.0	1.3(-5)

an upper limit and a factor of hundred lower than the solar value as a lower limit. During Phase II, the temperature rises fast and it reaches a maximum of 100 K.

2.2 Scenario 1: Grids B and C

In Grids B and C we assumed that the 0.12 pc final clump is inhomogeneous (See Figure 2). In Phase I, every depth point starts at 100 cm^{-3} and collapses until it reaches a final density, which varies from edge to centre of clump, according to the density law derived by Tafalla et al. (2002) for starless cores (and which we adopt):

$$n(r) = n_0 / [1 + (r/r_o)^\alpha] \quad (1)$$

where r_o and n_0 are the largest distance from the centre of the core and the peak density, respectively. α is the asymptotic power index and it is taken to be ~ 2.5 (see Table 2 in Tafalla et al. 2002). We divided our clump in 6

shells differing in density (n_f), visual extinction (A_V), and distance from the (future) outflow. Table 2 shows the parameters for each of the shells and Figure 2 gives a simplified graphical representation of the clump/outflow system (not to scale). In Table 2, Column 2 lists the distance of the shell from the edge, and Column 3 lists the final density for each shell. Phase I is halted when the final density is reached for each point.

Table 3 shows the details of the several models belonging to Grids B and C. To start with, we ran Phase I for two different percentages of gas as ices in the mantles (B1 and B2 models and C1 and C2 models). B3 and B4 are similar to respectively B1 and B2 but we adopted a variation to the routes of hydrogenation for some species (See Section 3.3.2 for details).

In Phase 2, Grid B simulates the arrival of the outflow by allowing the clump to undergo a non-dissociative shock where the mantle of the grains is evaporated and where the temperature of the gas reaches 1000 K and stays at this temperature for a short period of time (100 yr or so, following Bergin et al. 1999), after which the clump cools down to 100 K. In Grid C, the arrival of the outflow is simulated by simply an increase of gas and dust temperature up to 100 K, with a subsequent evaporation of the grains which occurs either instantaneously (C1–C2) or via time-dependent evaporation (C3), as in Viti & Williams (1999). Both Grids were run for 10^5 years.

2.3 Scenario 2: Grid D

In Scenario 2, the formation of molecular clumps along a molecular outflow occurs as a direct consequence of the impact of the outflow on a dark molecular cloud. We adopt the density structure of Eq. 1 (Tafalla et al. 2002) for this Scenario. Phase I simulates the formation of a a single-point dark core from a diffuse medium ($n = 100 \text{ cm}^{-3}$) collapsing in free-fall until $n = 10^4 \text{ cm}^{-3}$ is reached. The chemistry arising in Scenario 2 is explored for a range of physical pa-

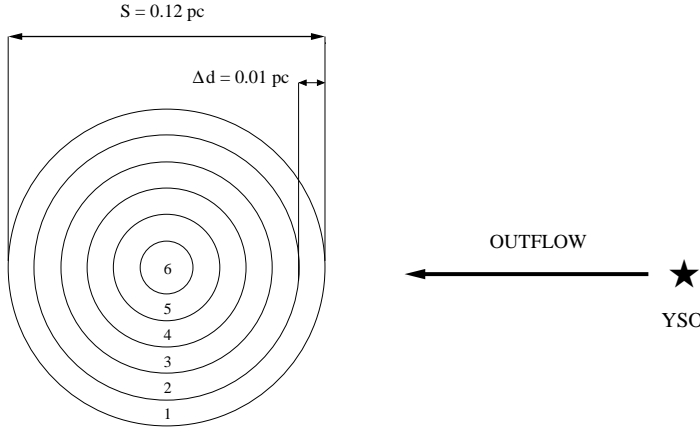


Figure 2. A schematic picture (not to scale) of the inhomogeneous clump modelled in Grids B, C and D. The chemical model is in 1-D, hence the chemistry is determined only along one symmetry axis. The geometry is then taken into consideration when estimating the column densities.

Table 2. Density structure for all Grids, apart from Grid A. The notation $a(b)$ signifies $a \times 10^b$. $d(\text{pc})$ is the distance between the mid-point of each shell and the edge of the clump (see Figure 1). n_f is the final density. A_V is the visual extinction between the outflow and the mid-point of each shell.

Shell	d (pc)	n_f (cm^{-3})	A_V (mags)
1	0.005	5.0(5)	10
2	0.015	6.4(5)	25
3	0.025	7.8(5)	45
4	0.035	9.0(5)	70
5	0.045	9.8(5)	95
6	0.055	1.0(6)	116

Table 3. Model Parameters for Grids B and C. The notation $a(b)$ signifies $a \times 10^b$. The model number is listed in Column 1; Columns 2, 3, 4 and 5 indicate whether the clump is pre-existing, the percentage of freeze-out, whether the gas is shocked, whether the evaporation has occurred instantaneously (I) or not (TD), respectively. The last column indicates whether a fraction of frozen H₂CO is converted into methanol - see Section 3.3.2 for details.

Model	FR (%)	Shock	Evaporation	$\text{H}_2\text{CO} \Rightarrow \text{CH}_3\text{OH}$
B1	40	yes	I	no
B2	60	yes	I	no
B3	60	yes	I	yes
B4	80	yes	I	yes
C1	40	no	I	no
C2	60	no	I	no
C3	60	no	TD	yes

rameters listed as Grid D (Table 4). We chose the freeze-out parameter so that the abundances of key species at the end of the collapse were consistent with observations of dark clouds (van Dishoeck 1998; cf. Bergin et al. 2002 for the CO

depletion). In Phase II we simulate the arrival of the outflow and the formation of high density clumps with final densities as in Table 2. We take as free parameters the outflow velocity and the initial distance of the dark cloud to the outflow. The models we have run are listed in Table 4; the ranges of velocities and distances were determined by considerations of the values derived for CB3 (Codella & Bachiller 1999). Note, however, that a high velocity outflow at a too close initial distance to the gas material (Models D2, D3, D6, D9) do not give the clump the time to form and reach the high densities considered. The density and temperature vary in the following way:

$$n(r) = n_i(r/r_i)^{-3/2} \quad (2)$$

and

$$T(r) = T_o(r/r_o)^{-0.4} \quad (3)$$

where r_i is the initial distance, T_o is an estimate of the hottest gas (~ 100 -200 K) and r_o is the closest (final) distance between the outflow and each shell within the clump that we are modelling, such that at $r = r_o$, $T(r) = T_o$. The initial distance varies of course from shell to shell; the distance between the edge of the clump (shell 1) and the outflow for each model is listed in Table 4. The temperature varies with time (and therefore with distance) as in Equation 3 (see Rowan-Robinson 1980).

Model D1 was also run with the addition of a post-shocked phase (with a temperature of 1000 K for 100 yrs, followed by cooling) during the formation of the clump, as in Grid B.

3 RESULTS

In Section 3.1 we give results from Grid A and briefly compare them to the observations. In Section 3.2 we present

Table 4. Model Parameters for Grid D. The model number is listed in Column 1; Column 2 and 3 are the velocity of the outflow and the initial distance between the cloud and the outflow, respectively.

Model	Velocity (km/s)	r (pc)
*D1	2	0.1
D2	20	0.1
D3	100	0.1
D4	2	0.2
D5	20	0.2
D6	100	0.2
D7	2	0.4
D8	20	0.4
D9	100	0.4

*Ran with two different temperature behaviours. See Section 2.3.

our results from Grids B, C and D while in Section 3.3 we compare them qualitatively with observations of the clumps detected along CB3 and L1157.

3.1 Grid A

In Table 5 we list the column densities at 10^5 yr, estimated from some of the models of Grid A as compared to the observations while Figure 3 shows the column densities of selected species as a function of time for some models.

From the table it is clear that the models from Grid A do not fit the observations. This is probably a consequence of the oversimplification introduced by the one-density component.

Nevertheless, general trends do emerge from this simple grid of models:

(i) a depleted sulphur initial abundance, rather than a solar one, is preferred; we note from our results that, apart from CS (whose abundance is mainly affected by the degree of depletion) other sulphur species, such as SO, are far too abundant if the initial sulphur is solar. This confirms previous studies (Ruffle et al. 1999; Viti et al. 2003).

(ii) Freeze-out on to grains must be effective at the densities considered here; we believe that at least half of the gas is depleted on to grain by the end of Phase I.

(iii) None of the species seem to be particularly affected by the type of collapse employed; for simplicity we will then adopt a free-fall collapse for the remainder of our Grids.

So far, we looked at the column densities at 10^5 yr, a kinematical age estimated by Codella & Bachiller (1999) for the clumps along CB3. However, this estimate may be easily off by over one order of magnitude, since it strongly depends on the assumed geometry of the outflow and it can thus vary in the $2 \cdot 10^4$ - $5 \cdot 10^5$ yr range (Codella & Bachiller 1999).

From Figure 3, we can see that certain species, such as CS, H_2CO , and SO_2 are very time-dependent; so for example the SO_2 column density is close to the observed one if the clump is less than 10^4 yr old, while CS is best matched at later times (see Model A9); if the density is closer to 10^6 cm^{-3} and sulphur initial abundance is low (models A7 and A9 in Figure 3) SO is reasonably matched before 3000 yr. These brief considerations underline the importance of constructing a clump with a density structure since not only we

notice that different species match observations at different densities, but also the degree of freeze out (which determines a great deal of the time dependent chemistry) is density dependent.

3.2 Grids B, C and D

As these grids share the same density structure, we discuss their trends together. Details of the parameters employed for grids B, C and D are listed in Tables 3 and 4 while the column densities for most models at 10^5 yr are listed in Table 6. Before commenting on whether or not they compare well with the observations (see Section 3.3), we look at the general trends as in the previous section.

3.2.1 Grid B vs. C

Table 6 shows that varying the percentage of gas as ices in mantles in Grid B (e.g B1 vs. B2) does not significantly affect the abundances of most species, while in Grid C the abundance of sulphur-bearing species can vary by up to one order of magnitude.

More significant differences are found between models of Grid B and those of Grid C, especially among the sulphur bearing species; this is not surprising as sulphur-bearing species are known to be good tracers of high temperature gas (e.g, Hatchell & Viti 2002; Hatchell et al. 1998). We find that CS is as much as two to three orders of magnitude more abundant in Grid B than in Grid C models while H_2S , SO and OCS vary by two orders of magnitude at most; H_2S is the driving species for the sulphur chemistry: it is enhanced on the grains during freeze out (via hydrogenation of sulphur) and it is then evaporated and dissociated during Phase II; since it is easily dissociated at high temperatures, it is, of course, more abundant in Grid C models (where the absence of a high temperature phase slows down its dissociation). A faster dissociation of H_2S in Grid B increases the abundance of other sulphur species, in particular we note OCS (an otherwise underabundant species). SO_2 , on the other hand, does not seem to be affected as much.

We conclude that, if the clump is pre-existing, then we should be able to easily discern whether it has undergone a high temperature phase or not using sulphur-species as tracers: moreover, if we assume that once the outflow has reached the clumps, non-dissociative shocks must occur, then sulphur bearing species can indeed be used as chemical clock in order to determine the age of the outflow/clump system, as proposed also by Codella & Bachiller (1999) and Bachiller et al. (2001) for the high-velocity outflowing gas.

3.2.2 Grids B, C vs. D

As expected, the differences between Grids B, C, and Grid D involve more species.

In particular, we find that, apart from sulphur bearing species, CH_3OH is a good tracer of the different scenarios. CH_3OH is not easily made in the gas-phase and is thought to be mainly formed on the grains via hydrogenation of a fraction of CO (Millar & Hatchell 1998) and possibly H_2CO . In a high temperature environment, CH_3OH has an alternative route of formation via water; in fact, we note from Table 6

Table 5. Column densities (in cm^{-2}) of selected species for some models from Grid A versus the column densities observed in CB3 (Column 6).

	A1	A4	A6	A8	Obs
CS	6.2(13)	1.2(13)	9.8(13)	1.1(14)	1.7(14)
H_2CO	1.1(16)	1.2(16)	3.5(16)	1.4(17)	5.9(14)
H_2S	1.8(17)	2.6(16)	1.1(18)	1.4(16)	1.9(14)
SO_2	4.1(16)	8.1(15)	1.1(19)	2.8(16)	5.6(14)
OCS	1.6(15)	2.5(14)	8.1(17)	1.6(14)	9.8(13)
SO	2.2(17)	3.2(16)	1.0(19)	3.8(15)	1.3(14)
CO	8.7(17)	8.7(17)	1.4(20)	9.8(18)	2.0(17)
CH_3OH	6.0(14)	8.0(14)	2.0(17)	2.9(16)	1.1(16)

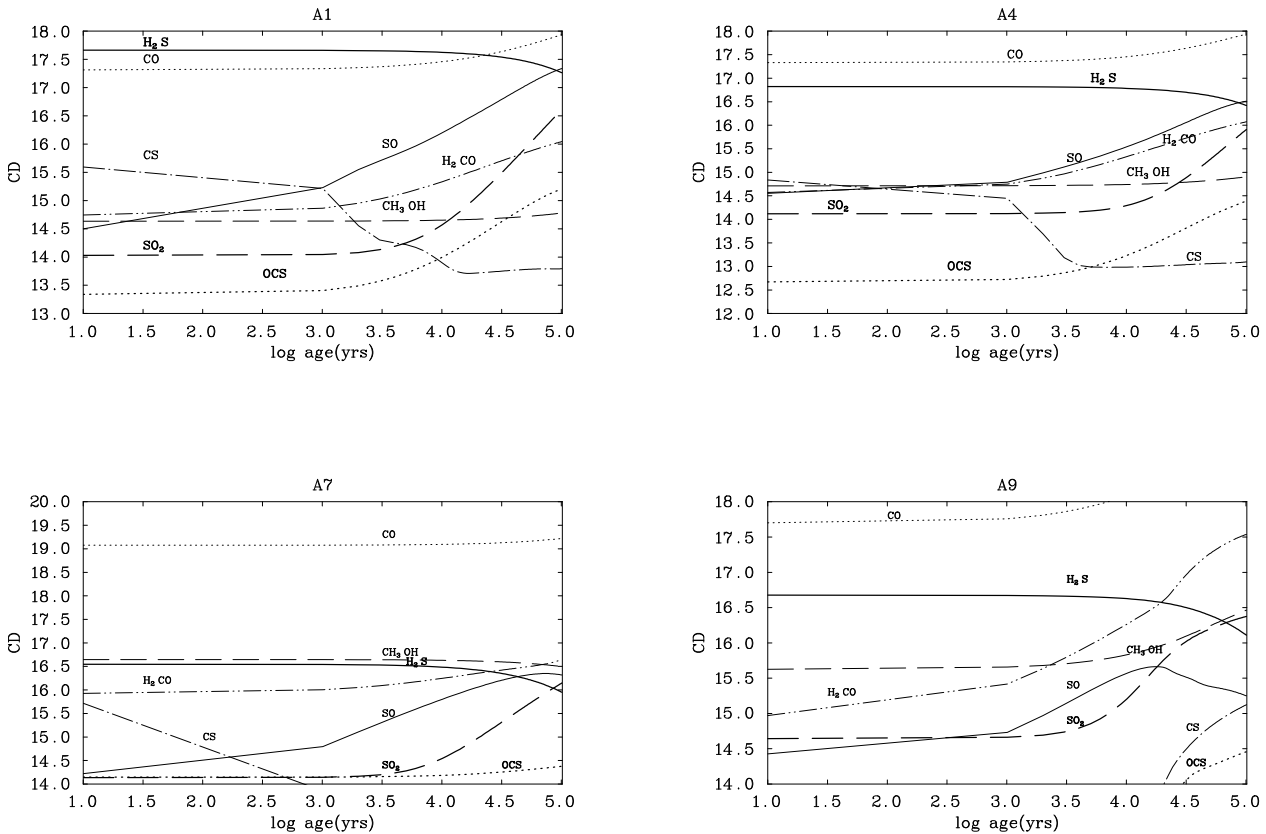


Figure 3. The column densities (in cm^{-3}) of a selection of species relative to hydrogen over time for selected models from Grid A.

Table 6. Column densities (in cm^{-2}) for selected models from Grids B, C, and D at $\sim 10^5$ yr vs Observed column densities

	B1	B2	B3	C1	C2	D1	D8	Obs
CS	1.66(15)	1.24(15)	4.76(15)	5.79(13)	1.60(14)	8.98(15)	9.64(15)	1.7(14)
H_2CO	2.32(17)	2.64(17)	1.73(17)	4.24(16)	1.20(17)	2.78(15)	2.74(15)	5.9(14)
H_2S	5.94(14)	5.97(14)	2.52(14)	4.00(15)	1.50(15)	4.90(13)	1.15(14)	1.9(14)
SO_2	5.64(15)	5.93(15)	2.59(15)	3.82(15)	6.56(15)	1.15(13)	2.13(13)	5.6(14)
OCS	1.61(14)	1.95(14)	6.15(13)	2.10(13)	2.71(13)	2.76(14)	2.77(14)	9.8(14)
SO	2.74(13)	3.21(13)	1.34(13)	8.89(14)	6.74(13)	2.43(13)	7.79(12)	1.3(14)
CO	1.11(18)	9.40(17)	1.16(18)	2.17(18)	1.56(18)	6.15(18)	6.32(18)	2.0(17)
CH_3OH	6.05(15)	6.40(15)	1.22(16)	5.48(15)	6.20(15)	2.12(14)	2.62(14)	1.1(16)

that, at equal freeze out, methanol is higher in B than in C models (cf B1 and C1), although at high freeze out they are comparable (cf B2 ad C2). This implies that a high abundance of CH_3OH depends more strongly on the amount of CO on the grains than on whether a high temperature phase has occurred.

For the same reason, Grid D models have a low abundance of CH_3OH as the formation of the clump took relatively little time, hence depletion and hydrogenation onto the grains was not very effective (Rawlings et al. 1992). If a high temperature phase is included for D1, the methanol abundance does indeed increase, but all the sulphur-bearing species increase by over one order of magnitude.

Methanol and sulphur-bearing species may therefore be the ideal candidates to determine whether the clumps originate as a consequence of the outflow or whether they are, at least partially, pre-existing.

3.3 Comparisons with observations

3.3.1 Derived gas parameters for CB3

In this section we briefly summarise how the gas parameters of the CB3 outflow have been derived from the IRAM 30-m observations (Codella & Bachiller 1999). For further details we refer the reader to the Codella & Bachiller (1999) paper.

The molecular outflow in CB3 is associated with at least four clumps located along the main axis. For the sake of clarity we calculated and used averaged values. The column density of SO, as well as the kinetic temperatures (T_{kin}) and the hydrogen density (n_{H_2}), have been derived by means of statistical-equilibrium LVG calculations. These two species, together with CH_3OH , have been observed in three emission lines. For CH_3OH a rotation diagram has been used to estimate the rotational temperature and its column densities. Gas density estimates have also been derived from the methanol emission patterns by measuring line intensity ratios. The column densities for the other molecules, observed in a single transition, have been estimated by assuming the lines optically thin and in LTE conditions, and by using standard partition functions. In this case, a temperature of 100 K has been adopted following the LVG indications for the clumps: the temperature uncertainty yields to an accuracy of the derived values within a factor of 10.

Note that with LVG calculations it is not possible to separate the effects on the excitation of the density and temperature. Moreover, LVG calculations do not take into account any correction due to the different beam filling factors at the three wavelengths of the observed transitions. As discussed by Codella & Bachiller (1999), if the source sizes were to be definitely smaller than the three beam widths, i.e. a sort of point-like source, the LVG code would lead to an overestimate of the excitation conditions: T_{kin} and n_{H_2} would be reduced by factors of about 2, while the column densities by a factor of 9.

The kinematical age of the outflow is estimated to be between 2×10^4 – 5×10^5 yrs, and it has been derived by comparing the positions of the farthest clumps, with respect to the driving source, assuming that the material travelled from the centre to its present location with a typical observed velocity of $\sim 2 \text{ km s}^{-1}$, and correcting for the projection effect, given an inclination to the plane of sky of 30° .

3.3.2 Model comparisons with CB3

Table 6 compares the column densities of Grids B, C and D with the observed values derived from the observations of Codella & Bachiller (1999), at 10^5 yr. Note that, unlike in the case of Grid A, the column density is calculated adding the contribution of each shell of the clump using the following formula:

$$N_i = \sum_s (X_i \times L \times n_s \times f_{i,s}) \quad (4)$$

where s is an index indicating the shell, X_i is the fractional abundance of species i , L is the length of each shell, n is the density of the shell, $f_{i,s}$ is the weighted beam dilution. In Grids B, C and D we do not need to approximate the inhomogeneity of the medium (as in Grid A) by multiplying the density by the visual extinction.

Also, since the age of the observed gas is uncertain (see Section 3.3.1), we also show in Figure 4 the behaviour of selected species as a function of time for some of the models listed in Table 6. The chemistries of some species, such as, in fact, the ones which show most discrepancies with the observations, are highly time dependent; for example, H_2CO , and some sulphur species, can be almost two orders of magnitude lower in abundances at early times.

At first sight, from Table 6, it appears that none of the models succeeds in reproducing *all* the observed column densities within the observed uncertainty (taken to be one order of magnitude, see Section 3.3.1).

However, we can see that Grid D fails to reproduce important species such as methanol and sulphur species and it is therefore the worse matching grid; Grid C improves over Grid D but still fails, in general, to match the observations for some sulphur species and, to a lesser extent, for methanol (see Section 3.2.2).

A first conclusion that can be made is therefore that *the chemically rich clumps along CB3 can not be formed completely by compression of the gas due to the advent of the outflow*. This, of course, implies that the high density of the clumps must have been reached before the advent of the outflow. This preliminary conclusion seems to be in contradiction with the conclusion by Arce & Goodman (2001, 2002) that the outflow clumps are the product of the sweeping up ambient gas. However, their assumption is that the ambient gas is homogeneous, at a density of $\sim 5 \times 10^3 \text{ cm}^{-3}$, and that the outflow will sweep-up a volume of $\sim 0.5 \text{ M}_\odot$, *maintaining* the same density of pre-existing cloud material – so, effectively, from a chemical point of view, the clump is indeed pre-existing the outflow/star system as the final density was reached without the intervention of the outflow. In this picture the morphology of the swept-up ambient gas and *not* its high density is a manifestation of the episodic nature of the outflow.

Grid B models seem to be the best, in particular B2 gives the closest match with observations, within half an order of magnitude (well within the observed error bars, see Section 3.3.1): apart from CO, all species are well matched for $t \geq 10,000$ yr, although H_2CO is definitely best matched at $t \leq 10,000$ yr. Although not obvious from Figure 4 (but evident from Table 6), the CO abundance in Grid B is \sim half the one in Grid C, due to the presence of a high temperature gas phase. However this difference did not increase

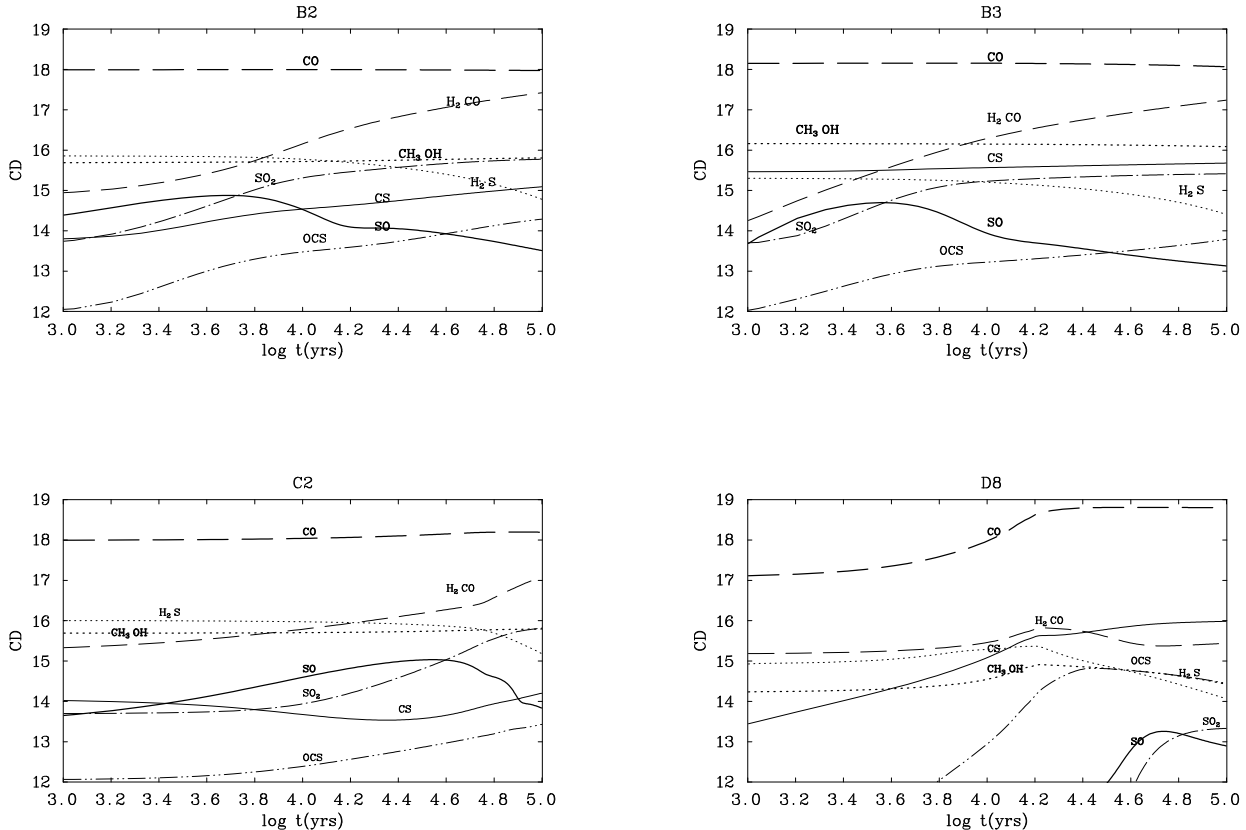


Figure 4. The column density of a selection of species over time for selected models from Grid B, C and D.

by increasing the high temperature phase to 500 yr (models not shown), as opposed to 100 yr as assumed in Grid B.

In general, we find that the theoretical abundance of H₂CO is overabundant with respect to the observations. One of the formation routes for H₂CO is the hydrogenation of CO, HCO and HCO⁺ on the grain mantles. We tried a model, B3 (also shown in Figure 4), similar to B2 but where i) frozen H₂CO is converted into methanol (a possible hydrogenation), ii) frozen HCO and HCO⁺ remain unaltered, upon depletion, iii) none of the carbon that freezes onto the grains hydrogenate into methane (unlike in previous models, where a percentage of carbon atoms became CH₄); the latter reaction is important because some of the H₂CO formed during the warm phase is formed by the reaction of water with CH₃ that comes from the dissociation of CH₄. We also computed a model, similar to B3, but with higher freeze out (B4, not shown in Figure 4). Although the final (at 10⁵ yr) fractional abundance of H₂CO is lower than in B1 or B2, we notice that in B3 and B4 the CS abundance is too high.

We can conclude therefore that the most likely scenario of the clumps observed along the outflow is a scenario where the *clumps are pre-existing, but undergo a high temperature phase (caused by a non-dissociative shock) when the outflow arrives, which leaves them altered in temperature for a period not longer than 5 × 10⁴ yr.*

3.3.3 The physical structure of the CB3 clumps

There are several reasons why Grid B models do not always quantitatively match the observations: for example, so far we have only looked at the total column density as coming from the whole clump. However, as shown from the results of Grid A, we know that the clumps must be formed by several density components; the density structure adopted here is believed to be representative of low-mass star-less cores (Tafalla et al. 2002) but it is likely that the density profile for the star-less, small clumps considered here have a different structure. It is therefore worth making some general considerations on the possibility that different species are emitted from different components of the gas.

Figure 5 shows, at two different epochs, the fractional abundances of selected species as a function of the density for the model B2. From this figure it is clear that if the clumps are as old as 10⁵ years the emission comes effectively only from a two-components density structure, one at $\sim 5 \times 10^5 \text{ cm}^{-3}$ and the other at $\sim 10^6 \text{ cm}^{-3}$. It may be that some gas comes from a lower density component but our ‘edge’ (lower) density was determined by imposing a upper density of 10^6 cm^{-3} (as derived by observations, see above). In fact, if we look at CO it seems as it is indeed the lower density component that is inconsistent with the observations. Note that although from this figure it seems as an homogeneous gas at 10^6 cm^{-3} would have matched the observations, this is not the case at earlier times, and overall

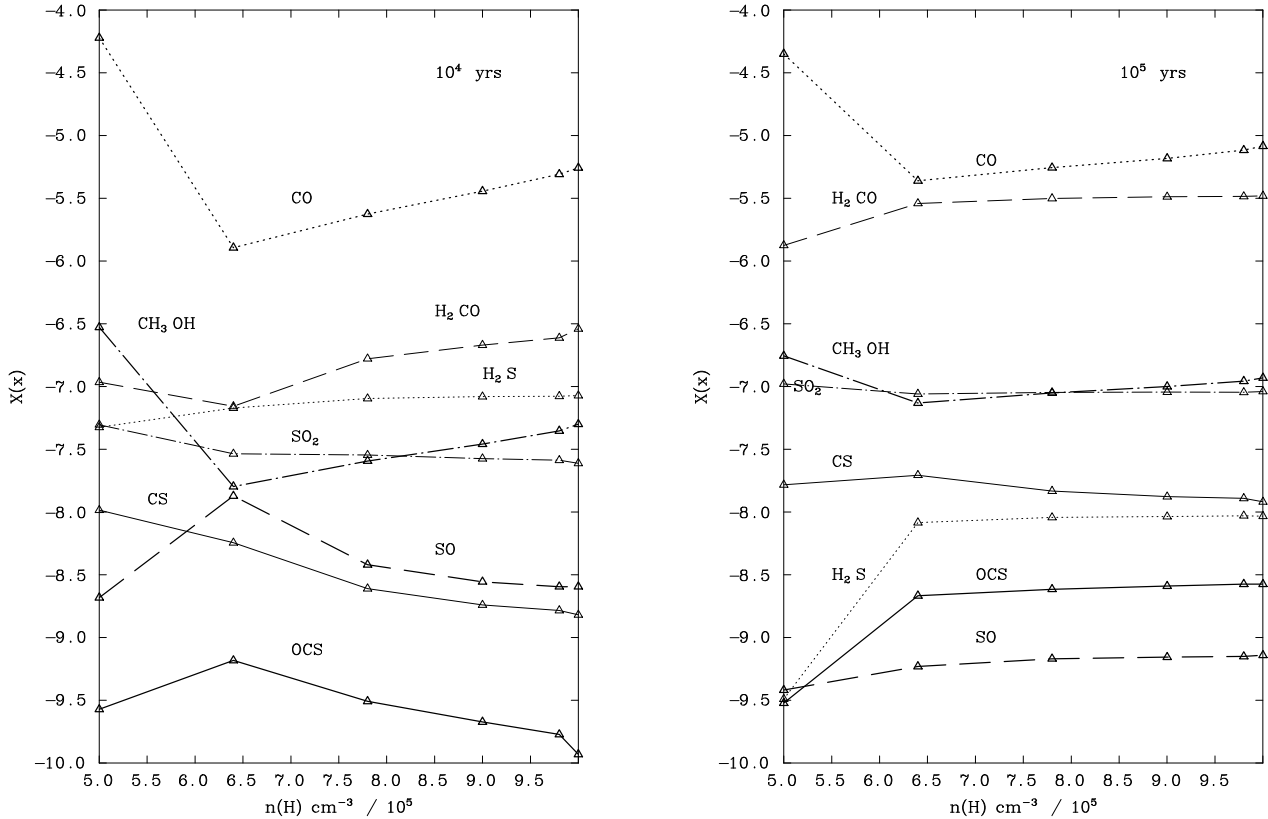


Figure 5. Fractional abundance of selected species as a function of density for Model B2 at 10,000 yr (left) and 10⁵ yr (right). The diamond marks indicate the densities at which each shell was computed. The points are joined for clarity.

during the collapse phase (which determines the grain surface chemistry), when the chemistry is much more density dependent.

A possibility is that the clumps observed are smaller than the size implied by the observations (and in fact 0.12 pc is an upper limit), but at higher density: this would imply a smaller A_V and therefore smaller column densities for the highest density components. General trends that can be derived from Figure 5 (overall left panel) are that:

- (i) CO and CH₃OH, and to a lesser extent CS and SO₂, are mainly emitted by the lower density components.
- (ii) H₂CO is slightly more abundant in the highest density parts.
- (iii) H₂S is more or less constant at early times, while SO and OCS seem to be highest at intermediate densities. At 10⁵ years, H₂S is mainly emitted from the highest density component.

Finally, it is not excluded that each clump observed by Codella & Bachiller (1999) does in fact contain substructures, not resolved in the single-dish observations because of the large distance of the source.

3.3.4 Another test case: L1157

Here we briefly compare our models with the chemical properties of the clumps observed in L1157. The associated out-

flow is driven by a low-mass YSO and will be subject of a future detailed study.

Bachiller et al. (2001) have mapped the bipolar outflow in several molecular emission lines and found chemical differentiation along the outflow. In particular they detect small (~ 0.04 pc) clumps in the southern lobe (B0–B2) which differ in densities and temperatures. If the origin of these clumps is similar to those observed along CB3, then their smaller size supports the possibility that the clumps along CB3 are smaller than the size implied by the observations due to the distance of the outflow (L1157 is only 440 pc away while CB3 is at 2500 pc). The best defined clump, called B1, has a density of $3\text{--}6 \times 10^5 \text{ cm}^{-3}$ and a kinetic temperature of $\sim 80 \text{ K}$, so, apart from its size, it is comparable to the clumps along CB3 and can therefore be briefly compared with our model results. Table 7 compares the column densities, recalculated (as if coming from a smaller size) with Equation 4, of our best-matching model (B2) at 10⁵ yr and of D2, with the derived column densities. Table 7 clearly shows that the match between B2 and the observations improves as the size of the clump is reduced. Grid D is still unable to match the methanol and most of the sulphur-bearing species confirming the results obtained for CB3.

Table 7. Column densities (in cm^{-2}) of selected species for B2 and D2 versus the observed column densities of the L1157 clumps.

	B2	D2	L1157
CS	1.15(14)	3.07(15)	2.7(14)
H_2CO	4.96(15)	8.57(14)	3-8(14)
H_2S	1.94(15)	5.53(13)	3.9(14)
SO_2	6.92(14)	6.40(12)	3.0(14)
OCS	1.00(13)	1.15(14)	5(13)
SO	1.04(14)	3.64(12)	3.5(14)
CO	3.28(17)	2.10(18)	1.4(17)
CH_3OH	1.72(15)	1.17(14)	0.5-2.6(15)

4 CONCLUSIONS

We have presented here a detailed time-dependent chemical model of the chemically rich clumps observed along outflows. This preliminary study was aimed at finding some observable tracers that could help us understanding the origin of the clumps with respect to the outflow. We also attempted a qualitative comparison of our models with some observations, in particular with the clumps observed along the CB3 outflow (Codella & Bachiller 1999). Despite large uncertainties in the mode of formation and several chemical assumptions we made, we believe that we are able to constrain some of physical and chemical parameters of the CB3 clumps. Our conclusions are:

1. The initial sulphur abundance of the gas forming the clump can not be solar. We find a depletion factor of ~ 100 , confirming the findings of other studies (Oppenheimer & Dalgarno, 1974; Ruffle et al. 1999).

2. A substantial freeze out must occur during the formation of the clump, regardless of its mode of formation.

3. Our models indicate that the most likely explanation for the outflow clumps is that they are pre-existing, meaning *only* that their density structure is, at least partly, formed prior of the advent of the outflow. This does *not* exclude the general explanation that the outflow clumps are mainly made of swept-up ambient gas and that therefore the clumps are an indication of the episodic nature of the outflows.

4. It is probable that, with the advent of the outflow, not only the temperature of the clumps increases and reaches the one observed, but the clumps also undergo a period of non-dissociative shock (and therefore high temperatures, ~ 1000 K).

5. The rich chemistry of the clumps observed along CB3, and L1157, seems to be a consequence of a pre-existing density enhancement (either uniform or already in clumps) and of its interaction with the outflow. The latter, most likely, shocks and accelerate the gas, and possibly, if episodic, induces its clumpiness. This is indicated by the high abundance of methanol and some of the sulphur-bearing species. In fact these molecules are formed by a combination of freeze out and surface reactions, and shocked chemistry: both most efficient when the outflow compresses already dense material at its passage.

6. We find that it is not possible for the outflow clumps to have a uniform high density - a density gradient is needed in order to account for the observed emission of most species.

7. CO, CH_3OH , CS and SO_2 are most likely emitted from the lower density components, while SO and OCS come from

an intermediate density component. This chemical stratification supports the findings of Bachiller et al. (2001).

8. At late times ($t > 10,000$ yr) H_2CO is *always* over-abundant by at least a couple of orders of magnitudes. This discrepancy is similar to that found for the clumps ahead of Herbig-Haro objects (Viti et al. 2003): these objects however do not share a common chemistry and we find no chemical reason why the abundance of H_2CO predicted by our models should be much larger than apparently observed. A possible explanation may be that the observed clumps are smaller than the size implied by the observations. In fact, when computing the theoretical column densities for smaller sizes (see Section 3.3.4), the match between theory and observations improves.

In conclusion, we suggest that interferometric observations of outflow clumps closer to us than CB3 are performed. This may reveal the real structure of these clumps and help constrain the models.

ACKNOWLEDGEMENTS

The authors are indebted to Prof D. A. Williams for useful conversations about clumpiness and for a critical reading of this revised version. SV and MB thank the Italian Space Agency for financial support. SV acknowledges individual financial support from a PPARC Advanced Fellowship. The authors are very grateful to the referee for comments and suggestions that substantially improved the manuscript.

REFERENCES

Arce H. G., & Goodman A. A., 2001, ApJ 554, 132
 Arce H. G., & Goodman A. A., 2002, ApJ 575, 928
 Bachiller R., 1996, ARA&A 34, 111
 Bachiller R., Martín-Pintado J., Fuente A., 1991, A&A 243, L21
 Bachiller R., Pérez Gutiérrez M., Kumar M. S. N., Tafalla M., 2001, A&A 372, 899
 Bergin E. A., Neufeld D. A., Melnick G. J., 1999, ApJ 499, 777
 Bergin E. A., Alves J., Huard T., Lada C. J., 2002, ApJ 570, L101
 Bourke T. L., Garay G., Lehtinen K. K., et al., 1997, ApJ 476, 781
 Charnley S. B., 1997, ApJ 481, 396
 Codella C., & Bachiller R., 1999, A&A 350, 659
 Dutrey A., Guilloteau S., Bachiller R., 1997, A&A 317, L55
 Falle S. A. E. G., & Hartquist T. W., 2002, MNRAS 329, 195
 Garrod R. T., Williams D. A., Hartquist T. W., Rawlings J. M. C., Viti S., 2003, A&A, submitted
 Hatchell J., Thompson M. A., Millar T. J., MacDonald G. H., 1998, A&A 338, 713
 Hatchell J., Viti S., 2002, A&A 381, L33
 Hester J. J., Stapelfeldt K. R., Scowen P. A., 1998, AJ 116, 372
 Le Teuff Y. H., Millar T. J., Markwick A. J., 2000, A&AS 146, 157
 Millar T. J., Farquhar P. R. A., Willacy K., 1997, A&AS 121, 139
 Millar T. J., & Hatchell J., 1998, Faraday Discussions n. 109, "Chemistry and Physics of Molecules and Grains in Space", p. 15
 Morata O., Girart J. M., Estalella R., 2003, A&A 397, 181
 Oppenheimer M., & Dalgarno A., 1974, ApJ 187, 231
 Rawlings J. M. C., Hartquist T. W., Menten K. M., Williams D. A., 1992, MNRAS 255, 471
 Richer J.S., Shepherd D.S., Cabrit S., Bachiller R., Churchwell E., 2000, in *Protostars and Planets IV*, ed. Mannings V., Boss A.P., Russell S.S., University of Arizona Press, p. 867

Rowan-Robinson M., 1980, *ApJS* 44, 403
Ruffle D. P., Hartquist T. W., Caselli P., Williams D. A., 1999,
MNRAS 306, 691
Tafalla M., Myers P. C., Caselli P., Walmsley C. M., Comito C.,
2002, *ApJ* 569, 815
van Dishoeck E. W., 1998, in *The Molecular Astrophysics of Stars
and Galaxies*, ed. T. W. Hartquist & D. A. Williams (Clarendon
Press, Oxford), 53
Viti S., & Williams D. A., 1999, *MNRAS* 310, 517
Viti S., Girart J. M., Garrod R., Williams D. A., Estalella R.,
2003, *A&A* 399, 187